Title

A Distal Arginine in Oxygen-Sensing Heme-PAS Domains Is Essential to Ligand Binding, Signal Transduction, and Structure †

Journal

Biochemistry, 42(25)

ISSN

0006-2960

Authors

Dunham, Christine M
Dioum, Elhadji M
Tuckerman, Jason R
et al.

Publication Date

2003-07-01

DOI

10.1021/bi0343370

Peer reviewed

A Distal Arginine in Oxygen-Sensing Heme-PAS Domains Is Essential to Ligand Binding, Signal Transduction, and Structure†

Christine M. Dunham,‡,§ Elhadji M. Dioum,§,|| Jason R. Tuckerman,|| Gonzalo Gonzalez,|| William G. Scott,‡ and Marie-Alda Gilles-Gonzalez*,||

Chemistry and Biochemistry Department, University of California, 236 Sinsheimer Labs, Santa Cruz, California 95064, and Department of Biochemistry, University of Texas Southwestern Medical Center, 5323 Harry Hines Boulevard, Dallas, Texas 75390-9038

Received February 28, 2003; Revised Manuscript Received May 12, 2003

ABSTRACT: To evaluate the contributions of the G_β-2 arginine to signal transduction in oxygen-sensing heme-PAS domains, we replaced this residue with alanine in *Bradyrhizobium japonicum* FixL and examined the results on heme-domain structure, ligand binding, and kinase regulation. In the isolated R220A *Bj*FixL heme-PAS domain, the iron−histidine bond was increased in length by 0.31 Å, the heme flattened even without a ligand, and the interaction of a presumed regulatory loop (the FG loop) with the helix of heme attachment was weakened. Binding of carbon monoxide was similar for ferrous *Bj*FixL and R220A *Bj*FixL. In contrast, the level of binding of oxygen was dramatically lower ($K_d \sim 1.5$ mM) for R220A *Bj*FixL, and this was manifested as 60- and 3-fold lower on- and off-rate constants, respectively. Binding of cyanide followed the same pattern as binding of oxygen. The catalytic activity was 3−4-fold higher in the "on-state" unliganded forms of R220A *Bj*FixL than in the corresponding *Bj*FixL species. Cyanide regulation of this activity was strongly impaired, but some inhibition was nevertheless preserved. Carbon monoxide and nitric oxide regulation, although weak in *Bj*FixL, were abolished from R220A *Bj*FixL. We conclude that the G_β-2 arginine assists in the binding of oxygen to *Bj*FixL but does not accomplish this by stabilizing the oxy form. This arginine is not absolutely required for regulation, although it is important for shifting a pre-existing kinase equilibrium toward the inactive state on binding of regulatory ligands. These findings support a regulatory model in which the heme-PAS domain operates as an ensemble that couples to the kinase rather than a mechanism driven by a single central switch.

In the signal-transducing proteins designated the heme-based sensors, a heme-binding domain regulates a neighboring transmitter (*1*). Members of a large category of these proteins have their heme in a PAS domain, a specialized sensory module of ∼130 residues (*2*). So far, this class includes a mammalian basic helix−loop−helix (bHLH) transcription factor and two different groups of microbial enzymes (*3*, *4*). The best known examples of the latter are the histidine protein kinase FixL and the cyclic nucleotide phosphodiesterases *Ax*PDEA1[1] and *Ec*Dos (*5*−*7*).

Whether associated with heme, other cofactors, or no cofactor, PAS domains have a conserved $\alpha-\beta$ three-dimensional fold (*2*). Members of the PAS family typically share little sequence homology (∼12% identical), but from this broad class, subgroups that are closely related can be identified. For the subgroup of bacterial heme-binding PAS domains, the amino acid sequences are ∼30% identical (*3*). They are most conserved in the regions that directly contact the heme (*8*). These include the α-helix (F_α) with the histidine that coordinates to the heme iron, a loop (FG) immediately following that helix, and two antiparallel β-strands (G_β and H_β) with the residues that come nearest to the bound ligand (Figure 1).

The G_β-2 arginine residue in the heme distal pocket of *Bradyrhizobium japonicum* FixL (Arg220) is notable for several reasons. It is conserved in all known FixL proteins, *Ax*PDEA1, and *Ec*Dos (*3*, *6*, *7*). It is the only polar residue

† This research was supported by U.S. Public Health Service Grant HL-64038, Award 2002-35318-12515 of the NRI Competitive Grants Program/USDA, National Science Foundation Grant MCB-0090994, and a Graduate Assistance in the Areas of National Need (GAANN) Grant to C.M.D.

* To whom correspondence should be addressed. E-mail: magg@biochem.swmed.edu.

‡ University of California.

§ These authors contributed equally to this work.

|| University of Texas Southwestern Medical Center.

[1] Abbreviations: *Bj*FixL, full-length *B. japonicum* FixL protein; *Bj*FixLH, *B. japonicum* FixL heme-binding domain; *Rm*FixLT, truncated *S. meliloti* FixL with heme-binding and kinase domains; *Ax*PDEA1, *Acetobacter xylinum* phosphodiesterase A1; *Ec*Dos, *E. coli* direct O_2 sensor protein; *Mt*DosH, *Methanobacterium thermoautotrophicum* Dos protein heme-binding domain; PAS, sensory domain with an $\alpha-\beta$ fold named after the eukaryotic proteins period, ARNT, and single-minded; heme-PAS, heme-binding PAS; Mb, myoglobin; SW Mb, sperm whale myoglobin; deoxy, Fe^{II} without ligand; met, Fe^{III} without ligand. For liganded heme proteins: $Fe^{II}CO$, carbonmonoxy; $Fe^{II}O_2$, oxy; $Fe^{II}NO$, nitrosyl; $Fe^{III}CN$, cyanomet; Fe^{III}imidazole, imidazolemet. For heme-PAS domains, which contain α-helices and β-strands, the alphanumeric code (e.g., G_β-2) gives the position in the protein and the type of secondary structure, together with residue location (*8*). For myoglobins and hemoglobins, the alphanumeric code (e.g., E7) refers to the position of amino acids in helices and turns in those proteins (*35*).

10.1021/bi0343370 CCC: $25.00
Published on Web 06/06/2003

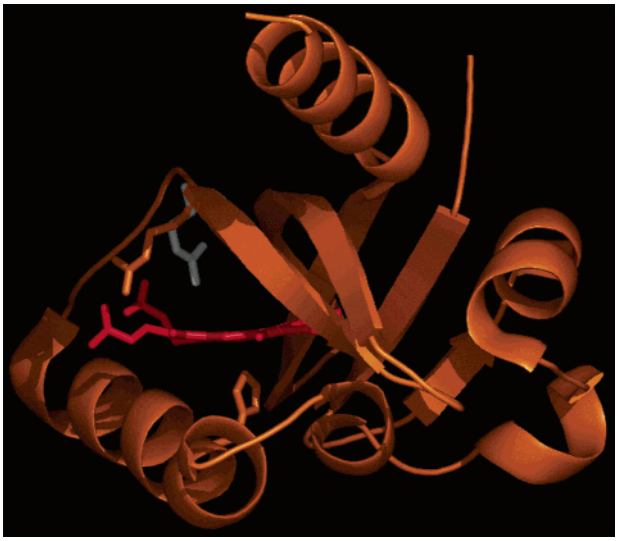

FIGURE 1: Two alternative orientations of the G_β-2 arginine in *Bj*FixL. A ribbon representation of the crystal structure of the ferric unliganded form of the normal protein, i.e., met-*Bj*FixLH, is shown (orange), together with stick representations of the heme (red), the proximal or F_α3 histidine (His200, orange), and the G_β-2 arginine (Arg220, orange) belonging to the same structure. The differently oriented G_β-2 arginine in a ligand-bound form, cyanomet-*Bj*FixLH, is superimposed (white). The names of the Protein Data Bank files are 1DRM for met-*Bj*FixLH and 1LT0 for cyanomet-*Bj*FixLH (*8*, *9*). This figure was created with the OS X native version of Pymol (*36*).

in the heme pockets of FixL proteins (*8*, *9*). In *Bj*FixL, this arginine is at the start of the distal G_β strand, just after the end of the FG loop, and is thus well poised to communicate to the FG loop the changes triggered by binding of ligands (Figure 1). A 2 Å displacement of the FG loop during binding of regulatory ligands has suggested that this loop plays a regulatory role (*8*). Finally, the G_β-2 arginine adopts alternative conformations in the unliganded "on" and the liganded "off" states of the *Bj*FixL heme-binding domain (Figure 1). Specifically, when the heme is unliganded, the guanido group forms a salt bridge to a heme propionate, but when the heme is bound to O_2 or CN^-, the guanido group enters the distal pocket to donate a hydrogen bond to the ligand (*9*).

The structural interaction of the G_β-2 arginine of *Bj*FixL with bound O_2 suggests that this residue stabilizes polar ligands in a manner analogous to that of the E10 arginine of *Aplysia limacina* myoglobin or the E7 histidine of sperm whale myoglobin (*10*−*12*). Interestingly, even with this guanido group present, the FixL dissociation equilibrium constants for binding of O_2 ($K_d \sim 50-140$ μM) are more than 50-fold higher than that of *A. limacina* myglobin (*1*, *11*). Instead, the affinities of FixL proteins fall within the range measured for hemes in entirely apolar media, such as free heme in benzene (*12*). Poor hydrogen bond donation from the G_β-2 arginine to O_2 or a low intrinsic affinity of the heme iron for O_2 may be responsible for the low affinities of FixL proteins despite their G_β-2 arginine.

In addition to the effects of the G_β-2 arginine on ligand binding, this residue is certain to influence signal transduction in FixL proteins. For all of the proteins examined so far, the ferrous forms are active if unliganded but inactive if bound to O_2 (*13*). The deoxy form can perform two reactions. If provided with ATP and the transcription factor FixJ, FixL catalyzes the phosphorylation of FixJ with a γ-phosphoryl group from the ATP (*5*, *14*, *15*). If given ATP alone, FixL transfers the ATP γ-phosphoryl group to a conserved histidine of its kinase domain (*5*, *16*, *17*). This latter "autophosphorylation" reaction is equally robust in deoxy- and met-FixL but is strongly inhibited by binding of O_2 to the ferrous form or CN^- to the ferric form (*15*, *18*). Although the *B. japonicum* and *Sinorhizobium meliloti* FixL/FixJ regulatory systems share these fundamental features, they differ in other important respects, including their affinities for heme ligands and precise regulatory targets (*1*, *19*−*21*). The enzymatic regulation has been studied most thoroughly for the *S. meliloti* FixL kinase, *Rm*FixLT, whereas the ligand-induced structural changes of the heme pocket have been observed only for the *B. japonicum* FixL heme-binding domain, *Bj*FixLH (*9*, *13*).

Here we examine for the first time the influence of heme ligands on the enzymatic turnover of *Bj*FixJ, as catalyzed by the full-length protein *Bj*FixL. We consider the role of the G_β-2 arginine residue in *Bj*FixL ligand binding, signal transduction, and heme-PAS domain structure.

MATERIALS AND METHODS

Genetic Manipulations. DNA fragments corresponding to full-length (codons 1−505) or the heme-PAS domain encoding region (codons 141−270) of *BjfixL* served as the templates for preparing *R220A BjfixL* and *R220A BjfixLH* by the QuickChange site-directed mutagenesis protocol (Stratagene). The mutation was confirmed by sequencing both strands of each DNA segment. Each final construct contained the gene segment under *tac*-promoter control on a plasmid conferring ampicillin resistance. This was transformed into *Escherichia coli* strain TG1. Procedures for overexpressing *R220A BjfixL* and *R220A BjfixLH* and purifying the corresponding proteins were essentially those previously described for *BjfixL* and *BjfixLH* (*1*, *8*).

Preparation of Liganded Derivatives. The deoxy form of *Bj*FixL was prepared by reducing the heme with dilute sodium dithionite and immediately removing this reducing agent by gel filtration on a Sephadex-G25 (Pharmacia) column inside of an anaerobic glovebox (Coy Laboratory Products Inc.). Oxy, carbonmonoxy, and nitrosyl forms of *Bj*FixL were obtained by mixing the deoxy form, in a solution containing 10 mM β-mercaptoethanol, with air (256 μM O_2), CO-saturated buffer (final concentration of >500 μM), and NO-saturated buffer (final concentration of >500 μM), respectively. Met-*Bj*FixL was prepared by oxidizing the protein with an equimolar solution of potassium ferricyanide. The cyanomet and imidazolemet forms were obtained by equilibrating the ferric protein with 10 mM KCN and 200 mM imidazole, respectively.

Ligand Binding. Absorption spectra were measured with a Cary 4000 UV−vis spectrophotometer (Varian Analytical Instruments, Walnut Creek, CA). Laser-flash photolysis and stopped-flow measurements were carried out with a LKS.60 laser kinetic spectrometer fitted with a Piestar stopped-flow drive unit (Applied Photophysics Ltd., Leatherhead, U.K.). For sample excitation, the LKS.60 spectrometer was coupled to a Quantel Brilliant B Nd:YAG laser with second-harmonic generation. Data were acquired with an Agilent 54830B digital oscilloscope for fast measurements or a 12-bit ADC card within the instrument workstation for slow measurements.

Association Rates. Rates of ligand association were measured for protein in 100 mM Tris-HCl (pH 8.0) at 25 °C at a wavelength of maximum difference between the starting and the final species. All protein concentrations are given as the total concentration of monomer. Ligands for the reactions were dissolved in 100 mM Tris-HCl (pH 8.0). Association of the ligand was monitored from the absorbance change at 426 nm for CO, 438 nm for O_2, 428 nm for NO, 427 nm for CN^-, and 419 nm for imidazole. For each ligand concentration, the apparent rate of association was measured at least three times. Rate constants were calculated from linear plots of k_{obs} versus ligand concentration.

For assessments of O_2 association to deoxy-*Bj*FixL, the rates of ligand binding were followed after rapidly mixing deoxy-*Bj*FixL (3−4 μM) with 80−410 μM O_2. For deoxy-R220A *Bj*FixL, the protein (40 μM) was equilibrated with 500, 700, or 1100 μM O_2, and the rates of O_2 rebinding were monitored from the change in absorbance at 440 nm after flash photolysis of the O_2. For assessment of CO or NO association, the rates of ligand binding were followed after rapidly mixing deoxy-*Bj*FixL or deoxy-R220A *Bj*FixL (2−4 μM) with 25−465 μM CO or 56−250 μM NO, respectively, in the stopped-flow spectrometer. Alternatively, the proteins were initially equilibrated with solutions of CO or NO, and the rate of rebinding of each ligand was followed after flash photolysis. For binding of ligands of ferric heme, the rates of association were followed after rapidly mixing each protein (3−6 μM) with 20−400 mM KCN or 1−10 mM imidazole in the stopped-flow spectrometer.

Dissociation Rates. Rates of ligand dissociation were measured for proteins in 100 mM Tris-HCl (pH 8.0) at 25 °C, as follows. The dissociation of O_2 from oxy-*Bj*FixL was monitored after mixing, in a stopped-flow spectrometer, 1 volume of oxy-*Bj*FixL (60 μM in 1.1 mM O_2) with 5 volumes of 2 mM sodium dithionite so that the dithionite instantaneously consumed any dissociated O_2. Carbon monoxide dissociation was assessed by monitoring formation of the nitrosyl form at 426 nm after adding a large excess of NO (500 μM) to the carbonmonoxy protein equilibrated with 50 μM CO. Cyanide dissociation was assessed by monitoring the formation of the imidazolemet form upon adding 200 mM imidazole to the cyanomet protein immediately after ridding the protein of free CN^- by gel filtration. Spectra of the cyanomet to imidazolemet transition were acquired from 1 min to 24 h after imidazole addition and showed clear isosbestic points. The cyanide dissociation rates were calculated from the changes in saturation over time, based on multiple linear regression of whole 350−700 nm absorption spectra.

Equilibrium Binding. The affinity of R220A *Bj*FixL for O_2 was directly measured by titrating the deoxy form with 250−1200 μM O_2 at 25 °C. To avoid autoxidation, each O_2 addition was done with a fresh solution of deoxy-R220A *Bj*FixL, and the absorption spectra were recorded immediately on mixing with O_2. The dissociation equilibrium constant was estimated from the changes in O_2 saturation based on multiple linear regression of whole spectra.

Phosphorylation Assays. The reaction mixtures contained 1−5 μM *Bj*FixL or R220A *Bj*FixL, a *Bj*FixJ:*Bj*FixL ratio of >25:1, and 1 mM ATP in "phosphorylation buffer" [50 mM Tris-HCl (pH 8.0), 50 mM KCl, 0.5 mM $MnCl_2$, and 5% ethylene glycol]. Reactions were started by adding the protein to the ATP (a mixture of [γ-^{32}P]ATP from Amersham Pharmacia Biotech and unlabeled ATP from Roche). At the indicated times, aliquots (~2.5−5 × 10^6 cpm) were withdrawn from the reaction solution and mixed with "stop buffer" [4 mM EDTA, 4% (w/v) sodium dodecyl sulfate, 0.5 M Tris-HCl (pH 6.8), 0.2 M NaCl, 50% glycerol, and 2% (v/v) β-mercaptoethanol]. The resulting amount of phospho-*Bj*FixJ was measured with a phosphorimager (Molecular Dynamics) after resolving the reaction products on 15% (w/v) polyacrylamide gels (*39*) and drying those gels. Under those conditions, the phospho-*Bj*FixJ accounted for more than 95% of the radiolabel in all proteins. Aliquots of radiolabeled ATP of known concentration and specific activity served as the standards.

Table 1: Data Collection and Refinement Statistics for Met-R220A *Bj*FixLH

data collection	
X-ray source	SSRL beamline 7-1
wavelength (Å)	1.08
resolution range (Å)	100−2.10
data cutoff [$\sigma(F)$]	none
completeness for range (highest-resolution shell) (%)	98.7 (94.0)
$I/\sigma(I)$ (highest-resolution shell)	5.6 (2.2)
multiplicity	4.1
no. of reflections	10416
R_{sym} (highest-resolution shell)	0.059 (0.032)
refinement	
refinement target	maximum likelihood
cross-validation method	throughout
R_{free} value test set selection	random
R	0.251
R_{free}	0.287
mean B (overall, Å^2)	49.6
rms deviation from ideal values	
bond lengths (Å)	0.007
bond angles (deg)	1.3

Crystallization and Collection of Diffraction Data. Crystals of R220A *Bj*FixLH were grown from 0.9 mM protein in 4.0−4.5 M NaCl, 5% 2-methyl-2,4-pentanediol (v/v), and 50 mM Hepes (pH 7.5), as reported previously for *Bj*FixLH (*8*). The protein solution (5 μL) was mixed with mother liquor (5 μL) and equilibrated in sitting drops against a 0.7 mL reservoir at 4 °C. Within 1−2 weeks, the crystals grew to their largest dimensions (0.3 mm × 0.3 mm × 0.3 mm). Immediately before the diffraction data were collected, the crystals were gradually equilibrated with 20% glycerol as a cryoprotectant. The cryoprotected crystals were rapidly frozen in a stream of nitrogen at 100 K. Diffraction data were collected on a Mar detector at the Stanford Synchrotron Radiation Laboratory (SSRL) on beamline 7-1. Data processing and reduction were performed with Mosflm and the CCP4 suite (*22*). Collection and processing statistics are summarized in Table 1.

Structure Determination and Refinement. To create a starting model from the original met-*Bj*FixL structure (PDB entry 1DRM), initial rigid-body refinement followed by conventional positional refinement (Powell minimization) in CNS 1.1 was performed (*23*). This starting model was further refined with a simulated annealing slow cooling molecular dynamics protocol followed by energy minimization and restrained temperature factor refinement in CNS 1.1. All model building, including substituting alanine for arginine at position 220, was performed in the O crystallographic

Table 2: Equilibrium Parameters for Binding of Ligands to Selected Heme Pockets with and without Polar Stabilization

protein	K_d (μM^{-1})		
	O_2	CO	CN^-
R220A *Bj*FixL[a]	1500	4.2	16
*Bj*FixL[b]	140	4.8	0.94
*Mt*DosH[c]	2.0	0.00035	
SW Mb[d]	0.83	0.037	1.3
H64F SW Mb[d]	130	0.012	920
Aplysia Mb[e]	1.0		
chelated heme in benzene[d]	67	0.0030	

[a] The K_d value for binding of O_2 was measured by titrating deoxy-R220A *Bj*FixL with O_2 at pH 8.0 and 25 °C. Also see Figure 2B. K_d values for binding of CO and CN^- were calculated from k_{on} and k_{off} at pH 8.0 and 25 °C. Details are given in Materials and Methods. [b] From ref *1*. [c] From ref *29*. [d] From refs *12* and *28*. [e] From ref *11*.

modeling program (*24*). From initial rounds of refinement, two differences from the starting model (1DRM) were apparent: the flattening of the heme and rotation of the proximal histidine (His200) around its Cβ−Cγ bond. Since model bias was a plausible reason for these observations, the initial refinements were repeated independently, deleting both histidine 200 and the heme while allowing the rest of the protein to refine. Histidine 200 and the heme were rebuilt from the resulting $3F_o - F_c$ difference maps.

RESULTS

Binding of Ligands. The most dramatic differences between *Bj*FixL and R220A *Bj*FixL were in the binding of O_2 and CN^-. The O_2 affinity of ferrous R220A *Bj*FixL ($K_d \sim$ 1.5 mM) was the lowest affinity so far measured for a heme-binding PAS domain (Table 2). Only 35% saturation of this protein could be achieved even in 1 atm of pure O_2 (Figure 2). For R220A *Bj*FixL, the on- and off-rate constants for binding of O_2 were 60- and 3-fold lower, respectively, than the values measured for *Bj*FixL (Figure 3 and Table 3). Cyanide binding appeared to be similarly impaired. The affinity of ferric R220A *Bj*FixL for cyanide was ~20 times lower than that of ferric *Bj*FixL, and this low affinity was likewise manifested as a large deceleration of the on-rate (30-fold) countered by a small decrease in the off-rate (2-fold) (Tables 2 and 3). In contrast, ferrous *Bj*FixL and R220A *Bj*FixL were essentially indistinguishable in the parameters measured for binding of CO or NO (Table 3).

Catalysis of FixJ Phosphorylation. Whether ferrous or ferric, unliganded R220A *Bj*FixL was 3−4 times more active than *Bj*FixL (Table 4). To compare the enzymatic response to a ligand, it was essential to saturate each protein with that ligand. Thus, the regulation of ferric R220A *Bj*FixL by CN^- was readily assessed, but the low affinity of the ferrous form for O_2 ($K_d \sim$ 1.5 mM) and the near absence of the inhibited oxy form at any practical concentration of this ligand prevented measurement of the response to O_2. Saturation of the heme with CN^- caused only a modest drop (2-fold) in the activity of R220A *Bj*FixL, although this essentially abolished the activity of *Bj*FixL (50-fold inhibition). Regulation by CO and NO was also much weaker in R220A *Bj*FixL. Carbon monoxide or NO binding to ferrous *Bj*FixL reduced the enzymatic activity 2−3-fold. In contrast, carbonmonoxy and nitrosyl R220A *Bj*FixL were fully active. Imidazole was the sole ligand found to regulate R220A

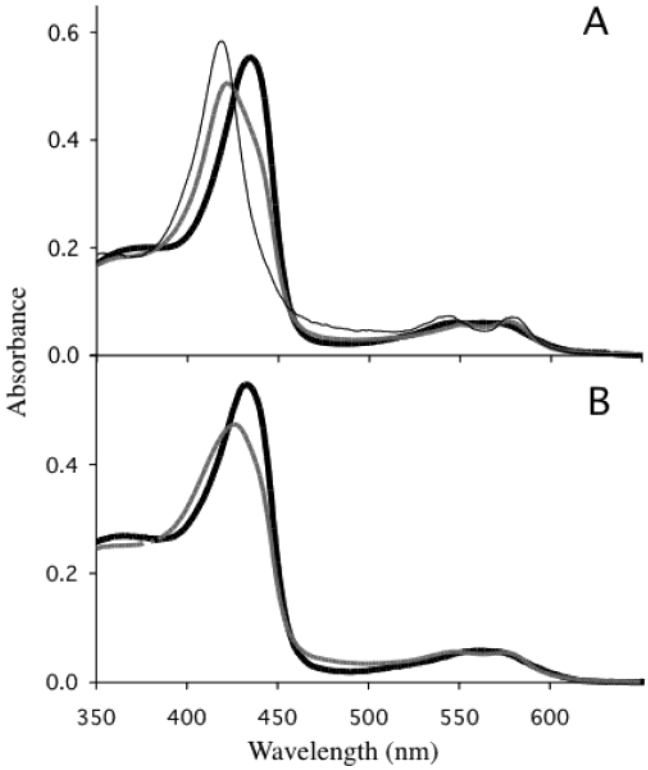

FIGURE 2: Saturation of R220A *Bj*FixL and *Bj*FixL proteins with O_2 at pH 8.0 and 25 °C. Part A compares the absorption spectra of ferrous *Bj*FixL exposed to no ligand (thick black line), 50% saturated in 140 μM O_2 (thick gray line), and fully saturated in 1100 μM O_2 (thin black line). Part B shows the absorption spectra of ferrous R220A *Bj*FixL exposed to no ligand (thick black line) or 35% saturated in 1100 μM O_2 (pale gray line). These figures agree with the equilibrium parameters in Table 2 and illustrate the stability of these species against autoxidation in 100 mM Tris-HCl and 10 mM β-mercaptoethanol (pH 8.0).

*Bj*FixL more stringently than *Bj*FixL. Saturation of the ferric forms with imidazole inhibited the activity of R220A *Bj*FixL 10-fold but that of *Bj*FixL only 5-fold. The results for *Bj*FixL were quite different from *Rm*FixLT, where all the ferric species were enzymatically inactive at FixJ phosphorylation (*15*).

Crystal Structure. Table 5 and Figures 4 and 5 highlight the main structural differences to accompany the Gβ-2 arginine-to-alanine substitution in met-*Bj*FixLH. These are (1) lengthening of the iron−histidine bond by 0.31 Å, (2) rotation of the imidazole ring of the proximal histidine (F_α3, or His200 in *Bj*FixL) 24° around its Cβ−Cγ torsion angle to an orientation less eclipsed by the pyrrole nitrogens, (3) tilting of the iron−histidine bond with respect to the heme plane, (4) flattening of the porphyrin, and (5) repositioning of both heme propionates.

Several key polar interactions between the heme and the protein were perturbed in met-R220A *Bj*FixLH (Figure 4 and Table 5). A salt bridge between the Gβ-2 arginine (Arg220) of *Bj*FixLH and the heme propionate 7 O2A atom had provided a direct link between the distal side of the heme and the porphyrin ring. Another salt bridge in *Bj*FixLH between the F_α9 arginine (Arg206) and the FG loop aspartate (Asp212) had tethered the end of α-helix F_α to the middle of the FG loop (*6*). In contrast, without the Gβ-2 arginine the heme propionate 7 carboxylate in R220A *Bj*FixLH became free to rotate 3° away from the heme plane relative

Table 3: Kinetic Parameters for Binding of Ligands to Selected Heme Pockets with and without Polar Stabilization

	O_2		CO		NO	CN^-		imidazole
protein	k_{on} (μM^{-1} s^{-1})	k_{off} (s^{-1})	k_{on} (μM^{-1} s^{-1})	k_{off} (s^{-1})	k_{on} (μM^{-1} s^{-1})	k_{on} (μM^{-1} s^{-1})	k_{off} (s^{-1})	k_{on} (mM^{-1} s^{-1})
R220A *Bj*FixL[a]	0.002 (0.004)	6.4	0.012	0.054	1.8	3.8×10^{-6}	6.3×10^{-5}	8.3
*Bj*FixL[b]	0.14	20	0.0083	0.040	2.0	1.1×10^{-4}	1.2×10^{-4}	4.9
*Mt*DosH[c]	6.2	12	1.7	0.00060		1.3×10^{-4}		74
SW Mb[d]	16	14	0.51	0.019	22	3.2×10^{-4}	4.0×10^{-4}	0.13
H64F SW Mb[d]	74	10000	4.5	0.054	57	1.2×10^{-7}	1.1×10^{-4}	1.4

[a] Binding of ligands to R220A *Bj*FixL occurred at 25 °C and pH 8.0. Values for k_{on} are calculated from linear plots of k_{obs} vs ligand concentration; values for k_{obs} are from kinetic traces of ligand binding after flash photolysis of the protein equilibrated with the ligand or after stopped-flow mixing of the ligand with the protein. Values for k_{off} are from kinetic traces of dissociation after displacement of the ligand with a competing ligand or redox agent. Details are given in Materials and Methods. Because of the low O_2 affinity of R220A *Bj*FixL and low quantum yield for flashing of O_2, the O_2 k_{on} from flash photolysis has an error of ±50% (Figure 3A); the O_2 k_{on} value in parentheses is calculated from experimentally determined K_d and k_{off} values and has an error of ±30%. For all other measurements, the average relative error is ±15%. [b] From ref *1*. Parameters for CN^- and imidazole binding are from this work. [c] From ref *29*. [d] From refs *28*, *37*, and *38*.

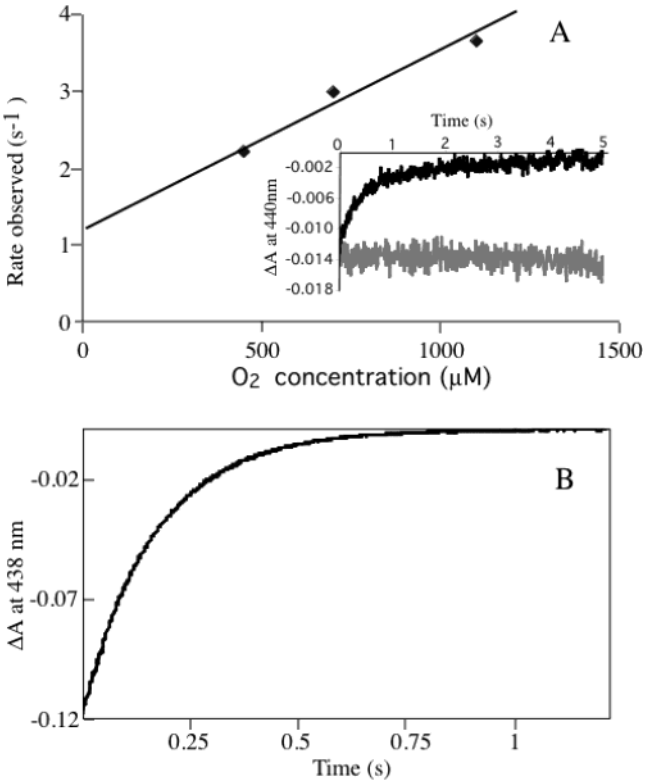

FIGURE 3: Kinetics of O_2 binding to R220A *Bj*FixL at pH 8.0 and 25 °C. Part A shows the rate of O_2 rebinding, as monitored from the change in absorbance at 440 nm, after flash photolysis of the O_2 from ferrous R220A *Bj*FixL (40 μM) equilibrated with 500, 700, and 1100 μM O_2 in 100 mM Tris-HCl and 10 mM β-mercaptoethanol (pH 8.0). The inset compares a kinetic trace after flash off of O_2 (black) to a trace obtained with blocking of the laser beam (gray). Note that the oxy form is serving as the zero. The stable baselines show that no other event occurred, and the amplitude of the reaction compared to the trace without flashing shows that the reaction was caught in its entirety. The k_{on} for binding of O_2 is estimated to be 0.002 μM^{-1} s^{-1}. Part B shows the dissociation of O_2 after mixing in a stopped-flow spectrometer 1 volume of oxy-R220A *Bj*FixL [60 μM, in 1.1 mM O_2 and 100 mM Tris-HCl (pH 8.0)] with 5 volumes of 2 mM sodium dithionite in 100 mM Tris-HCl (pH 8.0) at 25 °C. The k_{off} for binding of O_2 was determined to be 6.4 s^{-1}.

to its position in *Bj*FixLH. The F_α9 arginine of R220A *Bj*FixLH, which became poorly positioned for a salt bridge to the FG loop, engaged in two weaker hydrogen bonding interactions, one to the main chain carbonyl of the FG loop aspartate and the other to the heme propionate O2D through water. Overall, those changed interactions significantly disrupted communication of the heme status to α-helix F_α and the FG loop.

Table 4: Phosphorylation of *Bj*FixJ at pH 8.0 and 23 °C by *Bj*FixL Species Having Arginine or Alanine at the G_β-2 Position[a]

	turnover (h^{-1})[b]		inhibition factor[c]	
	*Bj*FixL	R220A *Bj*FixL	*Bj*FixL	R220A *Bj*FixL
ferrous species				
deoxy, Fe^{II}	26	75	1.0	1.0
oxy, $Fe^{II}O_2$	<0.1	nd[d]	>260	nd[d]
carbonmonoxy, $Fe^{II}CO$	8.2	65	3.2	1.1
nitrosyl, $Fe^{II}NO$	14	83	1.9	0.90
ferric species				
met, Fe^{III}	24	86	1.0	1.0
cyanomet, $Fe^{III}CN^-$	0.51	50	47	1.7
imidazolemet, Fe^{III}Imid	5.1	8.3	4.7	10

[a] Reactions were carried out with 1 mM [γ-^{32}P]ATP and a 25-fold excess of *Bj*FixJ to *Bj*FixL in 50 mM Tris-HCl, 50 mM KCl, 0.5 mM $MnCl_2$, and 5% ethylene glycol (pH 8.0) at 23 °C. The amount of phospho-*Bj*FixJ was measured with a phosphorimager after resolving the products by gel electrophoresis; this species accounted for more than 95% of the radiolabel in all proteins. [b] Average slope of the linear region of turnover (i.e., picomoles of P-FixJ per picomole of FixL) vs time curves, each curve including at least four points and giving an R^2 value of >0.985. [c] With respect to the unliganded derivative in the same oxidation state. [d] Under the conditions of the assay, R220A *Bj*FixL could not be saturated with O_2.

DISCUSSION

A Heme Iron Intrinsically Unreactive toward Binding of O_2. By omitting the contribution of the G_β-2 arginine to ligand binding, as in R220A *Bj*FixL, we were able to see that in *Bj*FixL the intrinsic affinity of the heme iron for O_2 is so low that any appreciable binding at standard temperature and pressure requires the G_β-2 arginine (Figure 2 and Table 2). Since the protein with a G_β-2 arginine binds O_2 10 times more strongly, this residue may be considered to supplement the O_2 coordination by ~2 kcal/mol. Although the arginine residue is near the bound O_2, the principal mechanism by which it assists binding cannot simply be hydrogen bonding to the ligand, as exemplified by the E7 histidine of vertebrate myoglobins. The principal effect of a loss of such a hydrogen bond by amino acid substitution should be a dramatic increase in the oxygen dissociation rate, as seen, for example, in the H64F substitution of SW Mb (Table 3) (*12*). The results in Figure 3B and Table 3 show that the dissociation rate of O_2 does not increase dramatically upon substitution of the G_β-2 arginine with alanine; in fact, this rate actually

Table 5: Distances (Å) for Changed Polar Interactions in the Heme Pocket of R220A *Bj*FixL Compared to *Bj*FixL

	met-R220A *Bj*FixL	met-*Bj*FixL	cyanomet-*Bj*FixL
direct heme interaction			
Fe−His200 NE2	2.44	2.13	2.10
Prop7 O1A−His214 ND1	2.76	2.78	2.64
Prop7 O1A−water	−[a]	2.85	2.81
Prop7 O2A−His214 ND1	3.05	3.07	3.36
Prop6 O1D−His214 N	3.18	3.23	2.86
Prop6 O1D−Ile215 N	3.02	2.90	3.50
Prop6 O1D−Ile216 N	3.01	3.36	3.95
Prop6 O2D−water	2.68	2.71	2.57
other heme pocket interactions			
Arg206 NH1−water	2.67	2.56	2.66
Arg206 NH2−Asp212 OD2	−[a]	3.08	−[a]
Arg206 NH2−Asp212 O	2.41	−[a]	2.65
Arg206 NH2−water	2.93	3.64	−[a]
Arg NE−water	2.54	−[a]	3.06

[a] Distances longer than 4.0 Å are excluded.

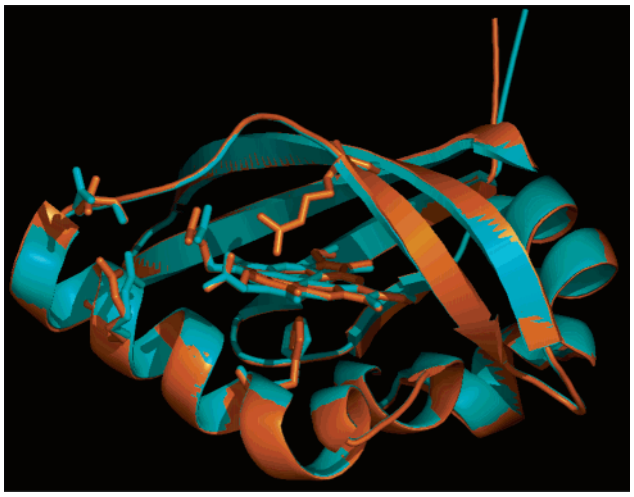

FIGURE 4: Changed heme environment in R220A *Bj*FixLH compared to *Bj*FixLH. Ribbon representation of met-*Bj*FixLH (orange) and met-R220A *Bj*FixLH (cyan) superimposed to highlight the differences between the two structures, which are mainly in the heme, the proximal or $F_\alpha 3$ histidine (His200), $F_\alpha 9$ arginine (Arg206), FG loop aspartate (Asp212), and distal G_β-2 arginine (Arg220). The G_β-2 arginine is replaced with alanine in the structure shown in cyan. This figure was created with the OS X native version of Pymol (*36*).

decreases ~3-fold. Instead, the stabilization of bound O_2 brought about by the G_β-2 arginine is manifested kinetically as a 60-fold acceleration of O_2 association. There is no plausible mechanism for such an acceleration by hydrogen bonding. Since O_2 is apolar until after it binds to heme iron, polar interactions can directly affect only the rate of O_2 dissociation but not its association.

Proximal Imidazole Orientation as a Factor in Heme Reactivity. Leghemoglobin provides another striking example of a heme pocket where the intrinsic reactivity of the heme iron supersedes any hydrogen bonding interactions with O_2 in determining the affinity. For Lb, the O_2 affinity is exceptionally high ($K_d \sim 0.040\ \mu M$), but this is clearly not due to donation of a hydrogen bond to bound O_2, since substitutions of the distal E7 histidine or B10 tyrosine with aliphatic residues hardly affect O_2 binding (*25*). Perutz and colleagues have suggested that in deoxy-Lb the barrier to O_2 association is lowered by the ability of the proximal-

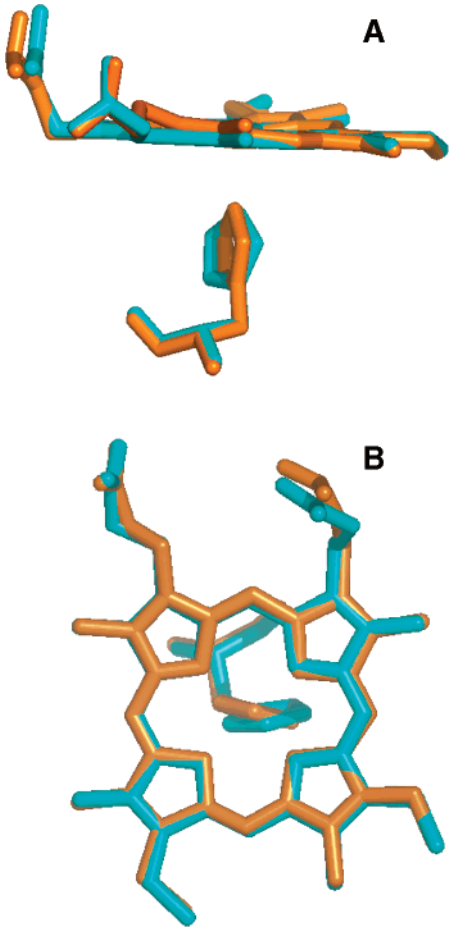

FIGURE 5: Reorientation of the proximal histidine in R220A *Bj*FixL. Part A shows an overlay of the hemes and proximal histidines (His200, or the $F_\alpha 3$ histidine) of met-R220A *Bj*FixLH (cyan) and met-*Bj*FixLH (orange). Differences are the flattening of the heme and rotation of proximal histidine in met-R220A *Bj*FixLH relative to met-*Bj*FixLH. Specifically, in met-*Bj*FixLH, the imidazole plane of the proximal histidine is roughly perpendicular to the heme plane, whereas in met-R220A *Bj*FixLH, there is a 24° twist around the $C\beta-C\gamma$ bond of the histidine. Part B shows the hemes and proximal histidines of met-R220A *Bj*FixLH (cyan) and met-*Bj*FixLH (orange) viewed perpendicularly to the heme plane, further emphasizing the 24° twist of the proximal histidine imidazole in met-R220A *Bj*FixLH (cyan) compared to met-*Bj*FixLH (orange). This rotation of the proximal histidine aligns the imidazole in met-R220A *Bj*FixLH in a more staggered position relative to the pyrrole nitrogens than the imidazole in met-*Bj*FixLH. This figure was created with the OS X native version of Pymol (*36*).

histidine imidazole to adopt a staggered conformation that minimizes steric hindrance from the pyrrole nitrogens and maximizes $\pi-\pi$ electron donation (*26*). One prediction of this hypothesis is that a staggered conformation of the imidazole in the unliganded form of a protein should enhance the affinity for O_2. Interestingly, in *Bj*FixL, the proximal histidine is staggered with respect to the pyrrole nitrogens, and in R220A *Bj*FixL, this histidine is even more staggered due to the 24° rotation of the imidazole ring from its position in *Bj*FixL (Figure 5). Thus, the Perutz hypothesis in its current form cannot explain why *Bj*FixL has a low affinity for O_2, and R220A *Bj*FixL has an even lower affinity. Perhaps a more significant difference between the proximal histidine in Lb and the one in Mb or *Bj*FixL is the vastly greater mobility of this histidine in Lb. Indeed, alternative conformations of the proximal histidine have never been

reported for mammalian Mbs and are not observed for either *Bj*FixL or R220A *Bj*FixL, but they are evident from NMR and even X-ray spectroscopic analyses of Lb (*25*−*27*). We therefore propose that the rotational freedom of the proximal-histidine imidazole, rather than the initial position of that imidazole, is a better determinant of the intrinsic reactivity of the iron atom in heme proteins.

How Does the G_β-2 Arginine Assist Binding of O_2 and Cyanide to BjFixL? As a heme ligand, cyanide is expected to enter and exit the hydrophobic heme pocket principally as the neutral HCN form, but it must be deprotonated to the CN^- form to coordinate to the heme iron (*28*). Thus, the kinetics of cyanide association with mammalian myoglobins are dominated by the rate of deprotonation of HCN inside the heme pocket; likewise, the rate of cyanide dissociation is dominated by the rate of reprotonation of the bound CN^-. The parameters for binding of cyanide to R220A *Bj*FixL and *Bj*FixL suggest that an "arginine-shuttle" mechanism could easily catalyze the association and dissociation of this ligand, in effect escorting the negatively charged cyanide ion into and out of the apolar heme pocket (Table 3).

Such an arginine-shuttle mechanism could not operate for O_2 because molecular oxygen is neutral and apolar. Since there can be no direct interaction of arginine with O_2 to influence the association rate, the effect of a distal arginine on O_2 association must be exerted via some other moiety, probably the heme. The low affinity of R220A *Bj*FixL for O_2 could be fully ascribed if we suppose that in *Bj*FixL the G_β-2 arginine assists O_2 binding by destabilizing the unliganded state (Table 2). In considering the factors that influence the affinity of heme proteins for ligands, one must bear in mind that the energies of *all* bonds broken or formed during ligand binding contribute to the total free energy of binding. Thus, the reactivity of the heme iron is influenced not only by the groups that directly contact the ligand but also by all other groups that change their interactions during binding. The heme carboxylates clearly fall in the latter category. In many heme proteins, including *Bj*FixL, the heme propionates are forced to shift their orientation with changes in the heme status, against the constraints imposed by the requirement to shield their charge within the hydrophobic matrix. During binding of O_2 to *Bj*FixL, a salt bridge is broken between the O2A atom of heme propionate 7 and the G_β-2 arginine, and a hydrogen bond is formed between this arginine residue and the bound ligand (*9*). Thus, the removal of the G_β-2 guanido group causes the loss of polar interactions not only with O_2 but also with heme propionate 7 (Figures 1 and 4). Interestingly, the structural changes of the ferrous heme pocket during binding of O_2 parallel the response of the ferric species during binding of CN^- but are not seen for CO or NO (*9*). Though the proximity of the G_β-2 arginine to O_2 and CN^- is an obvious feature of these structures, it is probably more important to consider that this arginine could not approach the bound ligand without first breaking away from a heme propionate inside of a hydrophobic matrix (Figure 1). This destabilization of the unliganded form should contribute favorably to the total free energy of ligand binding.

Implications for Other O_2-Binding Heme-PAS Domains. The above observations on *Bj*FixL do not imply that a G_β-2 arginine should be an expected feature of all O_2-binding heme-PAS domains. *Mt*DosH, for example, has a 70-fold greater affinity than *Bj*FixL for O_2, although this archaeal heme-PAS protein naturally has a threonine at its G_β-2 position (Table 2) (*29*). The necessity of a G_β-2 arginine for O_2 binding in *Bj*FixL is better explained by this protein possessing an O_2 binding mechanism that has evolved to operate with a G_β-2 guanido group as one of its integral parts.

Role of the G_β-2 Arginine in Signal Transduction. In R220A *Bj*FixL, the iron−histidine bond is 0.31 Å longer than in *Bj*FixL (Table 5). The distal side of the heme pocket is disconnected from the heme as a result of loss of the salt bridge to heme propionate 7, and the FG loop is similarly disengaged from ligand binding events as a result of rupture of the salt bridge between an FG loop carboxylate and the $F_\alpha 9$ arginine (Table 5 and Figure 4). Thus, a hallmark of the met-R220A *Bj*FixLH structure is a relaxation of coupling between the heme and the protein. The enhanced enzymatic activity of unliganded R220A *Bj*FixL compared to that of *Bj*FixL is most simply explained by a shift in the equilibrium between active and inactive states due to relaxation of coupling (Table 4). The kinase domains of several proteins of the two-component class, including *S. meliloti* FixL, are known to be active when detached from their accompanying sensory modules (*30*−*32*). This implies that the unregulated state for the kinase is the on-state and that regulation by the sensory domain consists of an inhibition. Our finding of a 3−4-fold higher kinase activity in R220A *Bj*FixL shows that even without a ligand, the equilibrium between active and inactive kinase favors the inactive form (Table 4). Binding of a regulatory ligand to the heme shifts this equilibrium yet farther toward the inactive state of the kinase (Table 4).

The broad rearrangements in the R220A *Bj*FixL heme pocket support a regulatory model in which the heme and protein residues act as an ensemble in coupling to the kinase, rather than a model in which the G_β-2 arginine works as the main conformational "switch" (Table 5 and Figures 4 and 5). If insertion of the G_β-2 guanido group into the heme distal pocket is necessary to stabilize the off-state, then substitution of this side chain with alanine should eliminate any regulatory advantage of O_2 or CN^- but should not alter CO regulation. Contrary to these predictions, CO regulation is clearly enhanced by the G_β-2 arginine, dropping from a 3-fold inhibition of the kinase in *Bj*FixL to no discernible inhibition of R220A *Bj*FixL (Table 4). Since R220A *Bj*FixL is more stringently inhibited by imidazole than by cyanide, the G_β-2 arginine might be viewed as granting cyanide some advantage in regulating *Bj*FixL. However, this residue is clearly not sufficient to achieve all the cyanide regulation. Although cyanide inhibition was 25-fold weaker in R220A *Bj*FixL, a 2-fold inhibition by this ligand persisted (Table 4).

Implications of the G_β-2 Substitution for Structural Models of Sensing. So far, there are three models that attempt to describe how an inhibitory heme ligand triggers a regulatory conformational change in *Bj*FixL. Specifically, all three models seek to define the event that triggers an FG loop displacement of approximately 2 Å.

(1) Steric-Displacement Model. The volume taken up by binding of the ligand causes displacement of distal side chains, leading to rearrangement of the heme pocket and movement of the FG loop (*33*).

(2) Propionate-Push Model. Flattening of the heme upon binding of the ligand leads to a shift in the positions of the

heme propionates, new polar interactions, and an outward push of the FG loop (*8*).

(3) Arginine-Insertion Model. Insertion of the G_β-2 arginine into the heme distal pocket to stabilize the ligand-bound off-state leads to new polar interactions and displacement of the FG loop (*9*).

The steric-displacement model would predict that ligands of the same volume should cause a similar inhibition and that distal side chain substitutions with bulkier residues should cause a perpetual inhibition. In fact, the inhibitory potency of ligands does not correlate with their size, and the inhibitory effects of distal residue substitutions do not correlate with their side chain volumes (Table 4) (*15*, *34*). The propionate-push model would predict that a more planar heme should lead to inactivation, since this model relies on the ligand-induced flattening of the heme to drive a conformational change. Our results showing that unliganded R220A *Bj*FixL is 3−4 times more active than *Bj*FixL, despite its planar heme, rule out this model (Figures 4 and 5A and Table 4). Neither the arginine-insertion nor the propionate-push model can explain why R220A *Bj*FixL continues to be inhibited by cyanide and is inhibited more strongly by imidazole (Table 4). Arginine insertion could not operate in R220A *Bj*FixL, since the G_β-2 arginine is absent from this protein. Our enzymatic studies, which provide the only direct measure of regulation, lead us to conclude that movement of the G_β-2 arginine cannot be the sole factor triggering a regulatory conformational change, although this arginine clearly contributes to regulation. These studies agree with the structure of R220A *Bj*FixLH, showing a heme pocket that responds as an ensemble to the removal of one of its side chains (Figures 4 and 5 and Table 5).

ACKNOWLEDGMENT

We thank Drs. John S. Olson and George B. Richter-Addo for thoughtful comments on the manuscript. We thank Ms. Kelly Krabill-Gerber for preparing mutant genes. Portions of this research were carried out at the Stanford Synchrotron Radiation Laboratory, a national user facility operated by Stanford University on behalf of the U.S. Department of Energy, Office of Basic Energy Sciences. The SSRL Structural Molecular Biology Program is supported by the Department of Energy, Office of Biological and Environmental Research, and by the National Institutes of Health, the National Center for Research Resources, the Biomedical Technology Program, and the National Institute of General Medical Sciences.

REFERENCES

1. Gilles-Gonzalez, M.-A., Gonzalez, G., Perutz, M. F., Kiger, L., Marden, M. C., and Poyart, C. (1994) *Biochemistry 33*, 8067−8073.
2. Taylor, B. L., and Zhulin, I. B. (1999) *Microbiol. Mol. Biol. Rev. 63*, 479−506.
3. Gilles-Gonzalez, M.-A. (2001) *IUBMB Life 51*, 165−173.
4. Dioum, E. M., Rutter, J., Tuckerman, J. R., Gonzalez, G., Gilles-Gonzalez, M.-A., and McKnight, S. L. (2002) *Science 298*, 2385−2387.
5. Gilles-Gonzalez, M.-A., Ditta, G. S., and Helinski, D. R. (1991) *Nature 350*, 170−172.
6. Chang, A. L., Tuckerman, J. R., Gonzalez, G., Mayer, R., Weinhouse, H., Volman, G., Amikam, D., Benziman, M., and Gilles-Gonzalez, M.-A. (2001) *Biochemistry 40*, 3420−3426.
7. Delgado-Nixon, V. M., Gonzalez, G., and Gilles-Gonzalez, M.-A. (2000) *Biochemistry 39*, 2685−2691.
8. Gong, W., Hao, B., Mansy, S. S., Gonzalez, G., Gilles-Gonzalez, M.-A., and Chan, M. K. (1998) *Proc. Natl. Acad. Sci. U.S.A. 95*, 15177−15182.
9. Hao, B., Isaza, C., Arndt, J., Soltis, M., and Chan, M. K. (2002) *Biochemistry 41*, 12952−12958.
10. Conti, E., Moser, C., Rizzi, M., Mattevi, A., Lionetti, C., Coda, A., Ascenzi, A., Brunori, M., and Bolognesi, M. (1993) *J. Mol. Biol. 233*, 498−508.
11. Cutruzzola, F., Travaglini Allocatelli, C., Brancaccio, A., and Brunori, M. (1996) *Biochem. J. 314*, 83−90.
12. Olson, J. S., and Phillips, G. N. (1997) *J. Biol. Inorg. Chem. 2*, 544−552.
13. Gilles-Gonzalez, M.-A. (2003) in *Oxygen Sensing: Responses and Adaptation to Hypoxia* (Lahiri, S., Semenza, G., and Prabhakar, N. R., Eds.) Vol. 175, pp 7−22, Marcel Dekker, New York.
14. Tuckerman, J. R., Gonzalo, G., and Gilles-Gonzalez, M.-A. (2001) *J. Mol. Biol. 308*, 449−455.
15. Tuckerman, J. R., Gonzalez, G., Dioum, E. M., and Gilles-Gonzalez, M.-A. (2002) *Biochemistry 41*, 6170−6177.
16. Gilles-Gonzalez, M.-A., and Gonzalez, G. (1993) *J. Biol. Chem. 268*, 16293−16297.
17. Lois, A. F., Weinstein, M., Ditta, G. S., and Helinski, D. R. (1993) *J. Biol. Chem. 268*, 4370−4375.
18. Gilles-Gonzalez, M.-A., Gonzalez, G., and Perutz, M. F. (1995) *Biochemistry 34*, 232−236.
19. David, M., Daveran, M.-L., Batut, J., Dedieu, A., Domergue, O., Ghai, J., Hertig, C., Boistard, P., and Kahn, D. (1988) *Cell 54*, 671−683.
20. Anthamatten, D., and Hennecke, H. (1991) *Mol. Gen. Genet. 225*, 38−48.
21. Nellen-Anthamatten, D., Rossi, P., Preisig, O., Kullik, I., Babst, M., Fischer, H. M., and Hennecke, H. (1998) *J. Bacteriol. 180*, 5251−5255.
22. Potterton, E., McNicholas, S., Krissinel, E., Cowtan, K., and Noble, M. (1994) *Acta Crystallogr. D50*, 760−763.
23. Brunger, A. T., et al. (1998) *Acta Crystallogr. D54*, 904−921.
24. Jones, T. A., Zhou, J. Y., Cowan, S. W., and Kjeldgaard, M. (1991) *Acta Crystallogr. A47*, 110−119.
25. Kundu, S., and Hargrove, M. S. (2003) *Proteins 50*, 239−248.
26. Harutyunyan, E. H., Safonova, T. N., Kuranova, I. P., Popov, A. N., Teplyakov, A. V., Obmolova, G. V., Rusakov, A. A., Vainshtein, B. K., Dodson, G. G., Wilson, J. C., and Perutz, M. F. (1995) *J. Mol. Biol. 251*, 104−115.
27. Narula, S. S., Dalvit, C., Appleby, C. A., and Wright, P. E. (1988) *Eur. J. Biochem. 178*, 419−435.
28. Dou, Y., Olson, J. S., Wilkinson, A. J., and Ikeda-Saito, M. (1996) *Biochemistry 35*, 7107−7113.
29. Tomita, T., Gonzalez, G., Chang, A. L., Ikeda-Saito, M., and Gilles-Gonzalez, M.-A. (2002) *Biochemistry 41*, 4819−4826.
30. Monson, E. K., Weinstein, M., Ditta, G. S., and Helinski, D. R. (1992) *Proc. Natl. Acad. Sci. U.S.A. 89*, 4280−4284.
31. Kamberov, E. S., Atkinson, M. R., Chandran, P., and Ninfa, A. J. (1994) *J. Biol. Chem. 269*, 28294−28299.
32. Park, H., Saha, S. K., and Inouye, M. (1998) *Proc. Natl. Acad. Sci. U.S.A. 95*, 6728−6732.
33. Perutz, M. F., Paoli, M., and Lesk, A. M. (1999) *Chem. Biol. 6*, 291−297.
34. Mukai, M., Nakamura, K., Nakamura, H., Iizuka, T., and Shiro, Y. (2000) *Biochemistry 39*, 13810−13816.
35. Perutz, M. F. (1970) *Nature 228*, 726−739.
36. DeLano, W. L. (2003) *The Pymol Molecular Graphics System*, DeLano Scientific, San Carlos, CA.
37. Quillin, M. L., Arduini, R. M., Olson, J. S., and Phillips, G. N., Jr. (1993) *J. Mol. Biol. 234*, 140−155.
38. Mansy, S. S., Olson, J. S., Gonzalez, G., and Gilles-Gonzalez, M.-A. (1998) *Biochemistry 37*, 12452−12457.
39. Laemmli, U. K. (1970) *Nature 227*, 680−685.

BI0343370